J. Condensed Matter Nucl. Sci. 29 (2019) 41–51

Research Article

High-temperature Calorimetric Measurements of Heat for Ni/H_2 Exothermic Reactions

Edward J. Beiting* and Dean Romein

TrusTech, Redondo Beach, CA 90278, USA

Abstract

Instrumentation developed to measure heat power from a high-temperature reactor for experimental trials lasting several weeks is being applied to gas-phase Ni/H_2 LENR. We developed a reactor that can maintain and record temperatures in excess of 1200°C while monitoring pressures exceeding 7 bar. This reactor is inserted into a flowing-fluid calorimeter that allows both temperature rise and flow rate of the cooling fluid to be redundantly measured by different physical principles. A computerized data acquisition system was written to automate the collection of more than 20 physical parameters with simultaneous numerical and dual graphical displays comprising both a strip chart and complete history of key parameters. Initial studies of the absorption of light hydrogen (H_2) by nickel are presented.
 ISSN 2227-3123

Keywords: Anomalous heat, Gas loading, Gas-phase LENR, High-temperature calorimetry, High-temperature cell, High-temperature hydrogen permeation, Hydrogen gas, Nickel-hydrogen absorption, Parkhomov replication

1. Introduction

A laboratory was built to study the heat release from the gas phase manifestation of the Anomalous Heat Effect (AHE aka LENR). We are studying two implementations of this manifestation. The first heats at low temperature (<400°C) nanoparticles of bimetals imbedded in micron-sized particles of refractory. The second heats nickel particles and hydrogen at high temperatures as described by Parkhomov [1,2] in Russia and by Qi et al. [3] in China.

2. Instrumentation

This second task requires the ability to maintain samples at temperatures up to 1300°C while monitoring temperature, pressure, and excess heat continuously for a period of weeks. Furthermore, the calorimeter is capable of accommodating kilowatt thermal power levels with accuracy and precision. The technology developed and initial results of the high temperature and high power measurements are described in this paper.

*Corresponding author. E-mail: ebeiting@ymail.com.

 ISSN 2227-3123

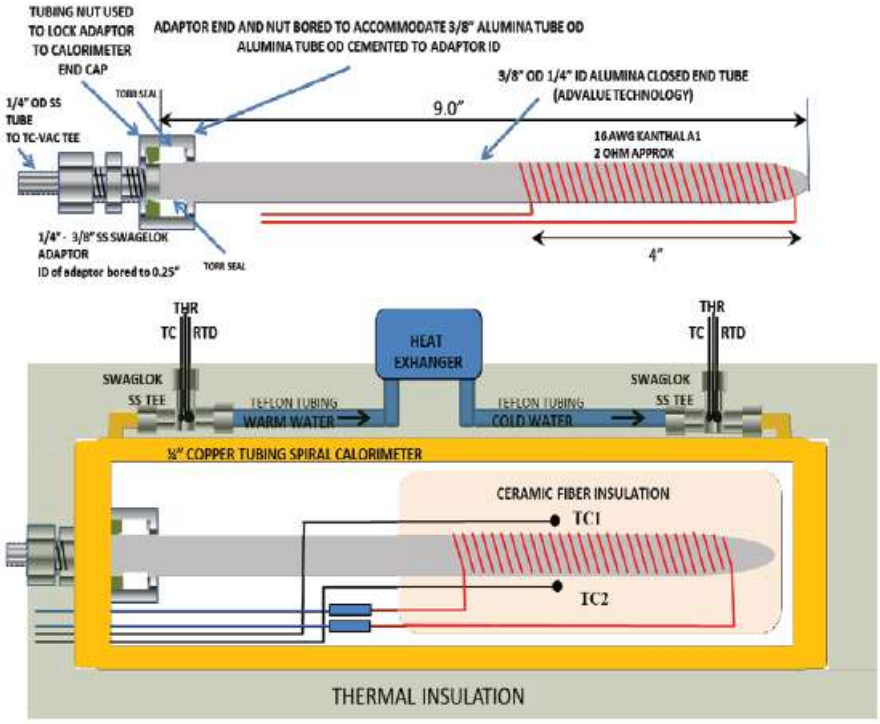

Figure 1. *Top*: Details of the high temperature reactor; *Bottom*: reactor in flowing fluid calorimeter. The heat exchanger circuit comprises a variable rate pump, a flow meter, a fan-forced radiator in a controlled temperature environment, and optionally a copper coil in a temperature-controlled refrigerated bath.

A drawing of the system is shown in Fig. 1. The design philosophy is to redundantly measure critical physical parameters using different physical principles. This calorimeter requires only two measured quantities, the volume flow rate ($\mathrm{d}V/\mathrm{d}t$) and temperature rise (ΔT), to measure the heat power (P), viz,

$$P = \rho c_{\mathrm{w}} \frac{\mathrm{d}V}{\mathrm{d}t} \Delta T, \tag{1}$$

where ρ and c_{w} are the density and mass specific heat capacity of the fluid, respectively. Typically this temperature difference is less than 10°C for an insulated reactor at a temperature of 1300°C and a water flow rate of less than 10 ml/s.

The inlet and outlet temperatures are registered using thermocouples (TCs), resistive thermal devices (RTDs), and thermistors. The flow rate is measured first by passing the fluid through a Hall effect flow meter that had an absolute accuracy of 1%. For a redundant flow measurement a second calorimeter can be connected in series; i.e. the flow from first passed through the second that houses the test reactor. The first calorimeter houses a heat source of known power and thus by measuring the temperature difference the flow rate could be calculated by Eq. (1).

A major task was to design a sealed container that heated the sample to high temperature and permitted the pressure in the volume to be monitored continuously. Its development resulted in a cell system that could be held continuously at a measured temperature of 1300°C for a period of weeks. Challenges were thermocouples that remained operational and accurate and heaters that did not fail after a few hundred hours.

The current reactor design is shown in top of Fig. 1 and its integration in the calorimeter is shown in bottom of Fig. 1. The length of the reactor's alumina tube [4] is chosen so that its unheated end remains below 100°C when the interior volume of the heated end is 1300°C. Empirical testing found that a 16 AWG Kanthal A1 wire spiral wrapped on the alumina tube is durable for the long trial periods. The method shown of sealing the ceramic tube to the stainless steel fitting was tested to a pressure of 8 bar.

Two external type-N thermocouples are to monitor the interior temperature of the reactor. Using external thermocouples have a number of advantages: there is no opportunity for the thermocouple metals to react with the reactant or their products; the thermocouple temperature is kept at a lower temperature (usually <1000°C) than that of the interior of the reactor thus increasing the thermocouple's life and accuracy; no high pressure/vacuum feed through is required; no high temperature electrical insulation isolating the thermocouple wire is required. Type-N thermocouples are more durable and accurate than type-K thermocouples at high temperatures.

The external thermocouples must be correlated with the interior temperatures of the reactor. This is done during a calibration run described below. The interior temperatures vary along the length of the tube under the spiral heater. The

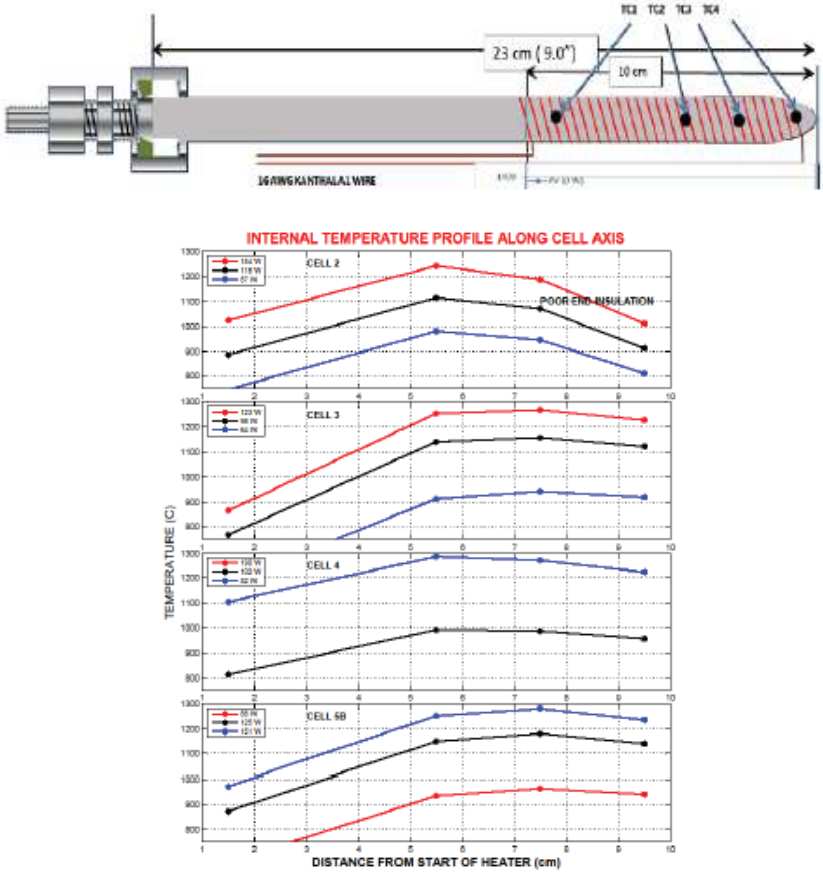

Figure 2. Temperature variation along the axis of cells

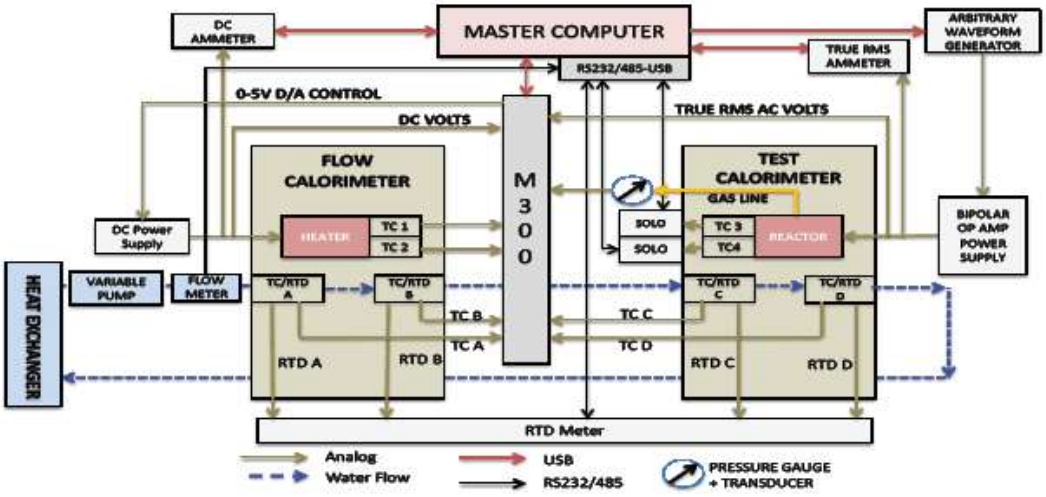

Figure 3. Functional diagram of the data acquisition system (DAQ).

variation is dependent on the insulation wrapped around the reactor. Figure 2 shows the temperature variation along the axis of four different cells taken with a four-thermocouple probe. The locations of the thermocouples are shown in the drawing at the top of the figure. If the end of the cell is poorly insulated, the temperature decreases significantly at the end as shown in the top plot.

Typically, the sample occupies about 3 cm of the 10 cm heated volume allowing it to be placed in the zone with the most uniform temperature using ceramic fiber spacers.

Figure 3 shows a functional diagram of an instrument with the optional calorimeter for the redundant flow rate measurement integrated into the data acquisition system (DAQ). A computer controls the experiment through USB ports using MATLAB® and its Instrument Control Toolbox software. Most measurements are made using a Rigol M300 DAQ system with 6.5 digit precision. The Rigol DM 3058E used as ammeters have 5.5 digit precision. SOLO 4824 temperature controllers monitor the reactor temperature for the type-N thermocouples. The output of a Rigol DG 1022 Arbitrary Waveform Generator is amplified by a Kepco BiPolar Operation Amplifier Power Supply when AC power heats the reactor. The calorimeter flow rate is measured using an Omega FMG81 flow meter with Laurel readout. A Define meter reads the RTDs. The water flow is controlled with a TCS MG1000S or MG2000S pulseless pump. Pt100 RTDs and thermocouples are purchased from Omega Engineering. Data were appended to a file every acquisition cycle with a maximum rate of 3 cycles/min, assuring that no data is lost if there were a system failure.

The AHE software was built for a class of experiments that start with initializing the software and then proceeds to collect experimental data over a long period of time. The experimental data collection is performed by a data acquisition loop that collects data from a suite of sensors connected to instruments. Every time through the acquisition loop, data are displayed to the operator using numeric displays and graphs. Some processing is performed to display values computed from the raw data. This processed data can also be displayed to the operator using numeric displays and graphs. Finally, the software allows experimental conditions, such as voltage to a power supply, to be changed either automatically by software or to be changed by operator actions.

The software has been built using object oriented programming principles that define software objects that are connected into a network of processing objects. The goal has been to build software that is maintainable and may be ported from one experiment platform to another experiment platform. Its architecture is shown in Fig. 4.

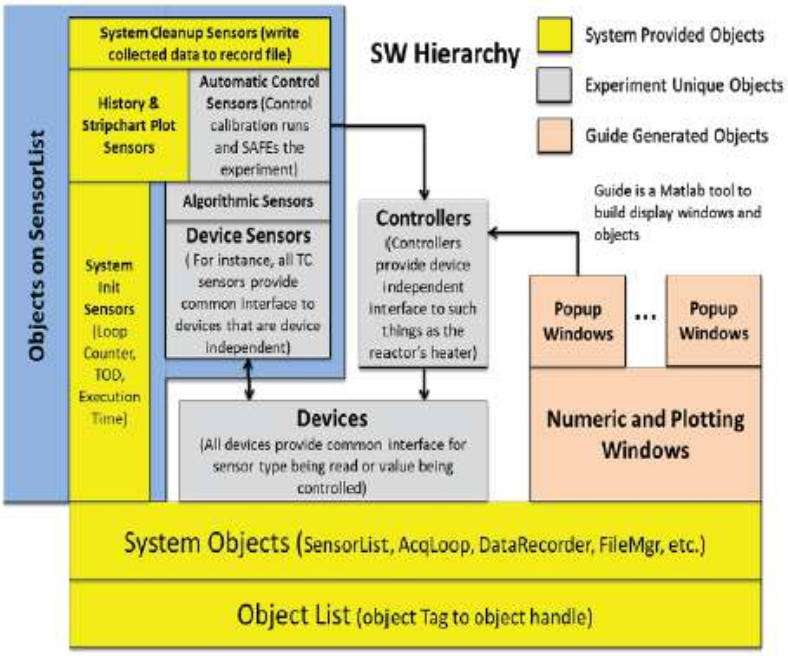

Figure 4. The software hierarchy.

The program runs in two phases. The first initializes all of the software objects and connects one object to another as needed. The second phase executes the data acquisition loop. The goal has been to build the software objects so that they are debugged once and then used as boxes that have certain properties that need to be defined during initialization. It should be possible to change no code except in the initialization functions that have been built for each set of software objects.

There are two types of objects used by the AHE software. The first displays objects provided by MATLAB. These objects include MATLAB figure, axes, and uicontrol objects (user interface controls), such as text or edit widgets. Each of these displays objects has the Tag property. The second are the user objects developed as part of the AHE software. These objects also have the Tag property. When a display object and a User object have the same tag, the AHE software automatically pairs the two during initialization phase so that the User object's data can be displayed during the acquisition loop. The MATLAB source code for this program is well documented and user manual is available. Its source code will be made available to interested parties.

The interactive two screen graphical inter-face is shown in Fig. 5. The axes of any of the plots are adjustable and operational parameters can be changed with push button controls.

The software automates the acquisition of the calibration data. An example of the data from a calibration sequence is shown in Fig. 6. This dense figure shows seven plots. From the top these are: (1) pressure (3×10^{-3} Torr here), (2) two interior and exterior temperatures in automated steps, (3) coolant flow rate, (4) the calorimeter entry temperatures measured with a thermocouple, RTD, and thermistor, (5) the triply redundant changes in calorimeter fluid temperatures, (6) the input power and triply redundant inferred powers, and (7) the measured excess power. The bottom plot showing the measured excess power requires explanation. The excess power during this trial is 0 W. Whenever the input power to the heater is changed, the temperature of the fluid (water in this case) flowing through the calorimeter begins to

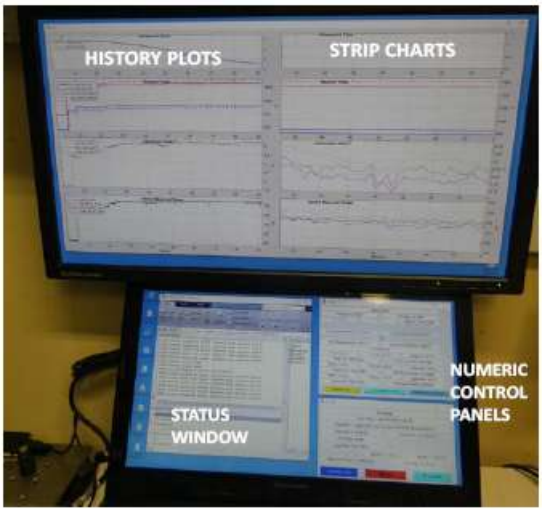

Figure 5. The two display monitors of the operating software.

change until it equilibrates. For the flow rate in this run (7.5 ml/s shown in the third plot), the equilibrium time is about 30 min. An increase in power results in a negative excursion (reading too low a power) and a decrease in power gives the positive excursion shown. A calibration parameter is adjusted for each temperature sensor (two are required for the thermistor) to give the accuracy shown in the bottom plot. The accuracy shown is about ± 0.5 W, which is better than 0.5% for the maximum input power of about 140 W.

The second plot from the top shows interior temperature registered by two of the interior thermocouples (red lines) and the temperatures registered by the two external thermocouples (blue lines). Third order polynomial fits of interior to exterior temperatures are used to infer the interior temperatures from measured external temperatures during a test run. This creates four inferred temperatures and the highest and lowest inferred values are display on the numeric panel in Fig. 5.

3. Initial Experimental Studies

Initial studies focused on replication of work of Parkhomov et al. [1,2]. We obtained three samples of Vale nickel powder labeled Type 123, Type SNP, and Type 255 [5]. Electron micrographs of these samples are shown in Fig. 7. Type 123 was chosen as most closely resembling that used by Parkhomov.

The sample tested was 1 g of Type 123 nickel powder and 0.1 g of $LiAlH_4$. Of several test trials, only one showed the characteristic pressure profile described by Parkhomov et al. These data are shown in Fig. 8. The first pressure rise occurred at below 200°C and the first pressure decrease at 250°C. Two additional steps to 550°C and 950°C induced the final pressure increases and taking the temperature to 1250°+C inducing the long pressure drop to sub-atmospheric at 65 h. No excess power was observed as seen in the bottom plot.

A similar inability to observe subsequent pressure drops after initial success was observed by Qi et al. [3] who did observe excess heat on the initial run. They attributed this behavior to nickel reaction with the atmosphere after their initially sealed container was left open. Our container of nickel was never sealed and was always exposed to the atmosphere.

In order to study the lack of pressure decrease (assumed to be nickel absorption) in subsequent trials, it was decided

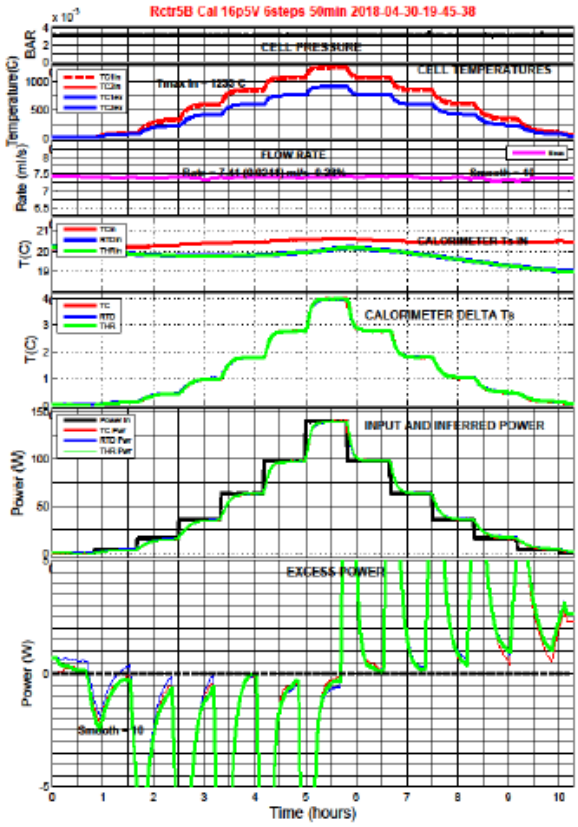

Figure 6. Example of calibration data.

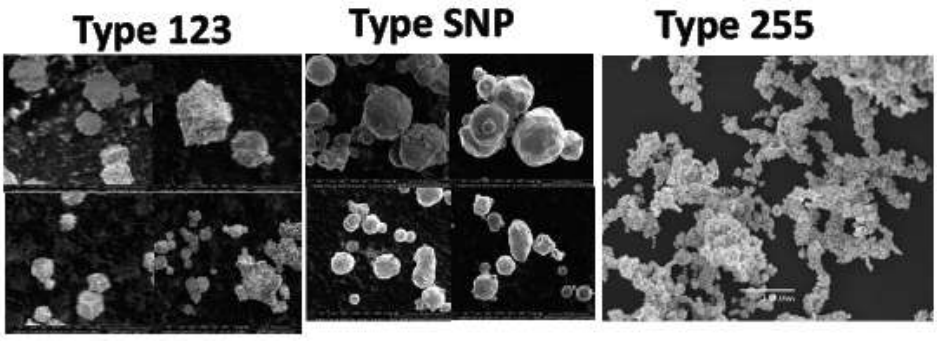

Figure 7. Electron micrographs of three types of Vale nickel powder.

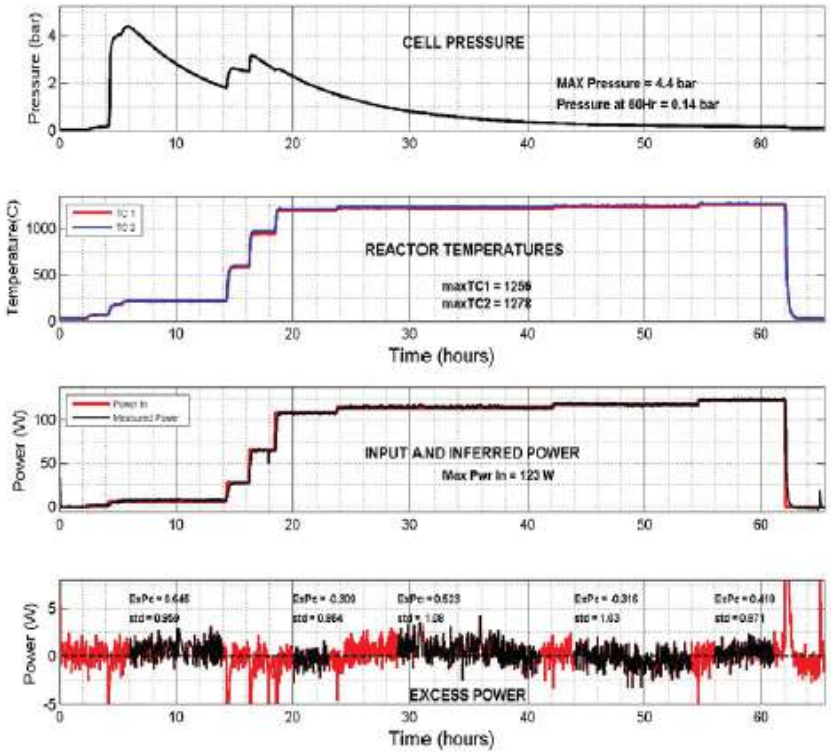

Figure 8. One-time pressure profile of a mixture of nickel powder and $LiAlH_4$.

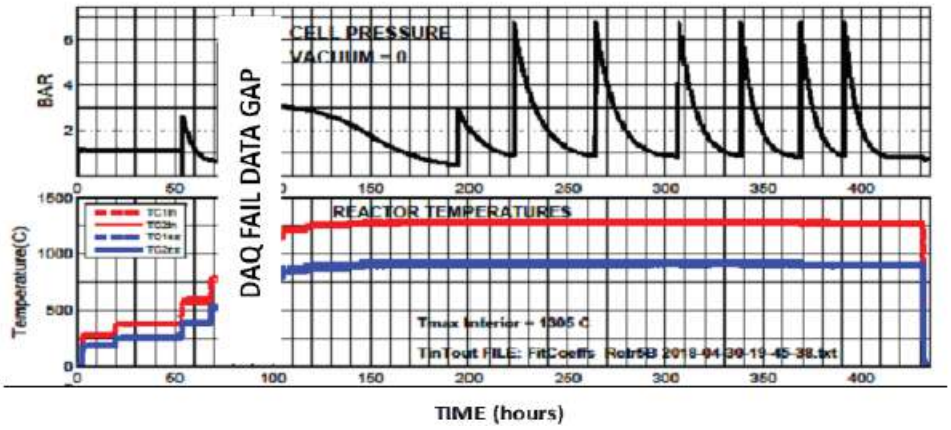

Figure 9. Data run interrupted by ICCF-21 conference.

Table 1. History of pressure changes in cell.

Moles Ni=0.034075			
Press No.	ΔP(bar)	H moles	H mole frac.
1	1.5	0.0028	0.0811
2	2.3	0.0042	0.1243
3	2	0.0037	0.1081
4	5.75	0.0106	0.3108
5	5.75	0.0106	0.3108
6	5.75	0.0106	0.3108
7	5.75	0.0106	0.3108
8	5.75	0.0106	0.3108
9	5.75	0.0106	0.3108
	Total=	0.0742	2.1781

to load the cell only with Vale 123 nickel and pressurize with pure hydrogen. The data from a 460 h (19 days) run shown in Fig. 9 were presented in the poster paper at ICCF-21. Subsequently, the cell was cooled and remained sealed at room temperature for three weeks when work was interrupted to attend the conference. After returning from the conference, the cell was reheated and re-pressurized to 5.75 bar and it again decreased to a sub-atmospheric pressure in a similar manner to that seen in the last six pressurization shown in Fig. 9. The total time this nickel sample was heated in the cell was 520 h (22 days) with 420 h (17.5 days) at a temperature above 1200°C. During these periods the cell was repeatedly pressurized with hydrogen as shown in these figures.

If one assumes that all the hydrogen is absorbed by the nickel in Fig. 9, the repeated pressurizations in Fig. 9 lead to the values presented in Table 1. This table, also presented at ICCF-21, shows an atomic H to atomic Ni mole fraction of a little less than 2.2 for the cumulative absorptions. Adding the additional post conference pressurization increases this mole fraction ratio to 2.5. Note that the pressure value in each pressurization is allowed to decrease to a sub-atmospheric value before re-pressurization in order to assure that there were no leaks to atmosphere in the system.

From Fig. 9 (and the subsequent pressurization) it is seen that the rate of hydrogen absorption increases as the assumed ratio of atomic H-to-nickel atom ratio reaches 2.5. Either nickel can absorb copious hydrogen at high temperature or hydrogen is lost via another mechanism, possibly permeating into or through the walls of the system.

To check this conjecture, a previously used cell that had been held at elevated temperatures for 150 h and temperatures above 1200°C for 70 h was reconfigured for a test. A new heater coil and insulation were installed and the empty cell (except for 3 cm of fiber insulation [6]) was installed in the calorimeter. This cell was then heated to an internal temperature of >1200°C for more than five days. During this period the cell was pressurized twice with 84 psig (6.7 bar) of H_2. The results of this test are shown in Fig. 10.

It is clear from the pressure curve (second from the top) in this figure that nickel is not required to give the pressure drops see in Fig. 9. The first pressurization was allowed to fall to 2 bar before re-pressurization but the second was allowed to fall well below atmospheric pressure (0.6 bar) before allowing the temperature to drop to ambient, reaching a minimum pressure of 0.56 bar before slowly increasing for the next 15 h. Subsequently, the cell was opened to atmosphere to check the calibration of the pressure transducer, which read 1.0089 bar for an accuracy of better than 1%.

The bottom two curves in Fig. 10 show the rates of the pressure drops. Note from the third curve the maximum depressurization rate of the first pressurization is -0.4 bar/h and the second is about –0.25 bar/h. From the bottom curve we note that the depressurization rate is approximately proportional to the pressure.

Because hydrogen is known to have a high permeation rate at high temperatures, the permeation rate was explored for both the stainless steel tubing and alumina of the system. Noting that 304 and 316 stainless steel have nearly the same permeation rate [7,8], we use the values given by [8] to calculate the permeation rate for the gas system of 25

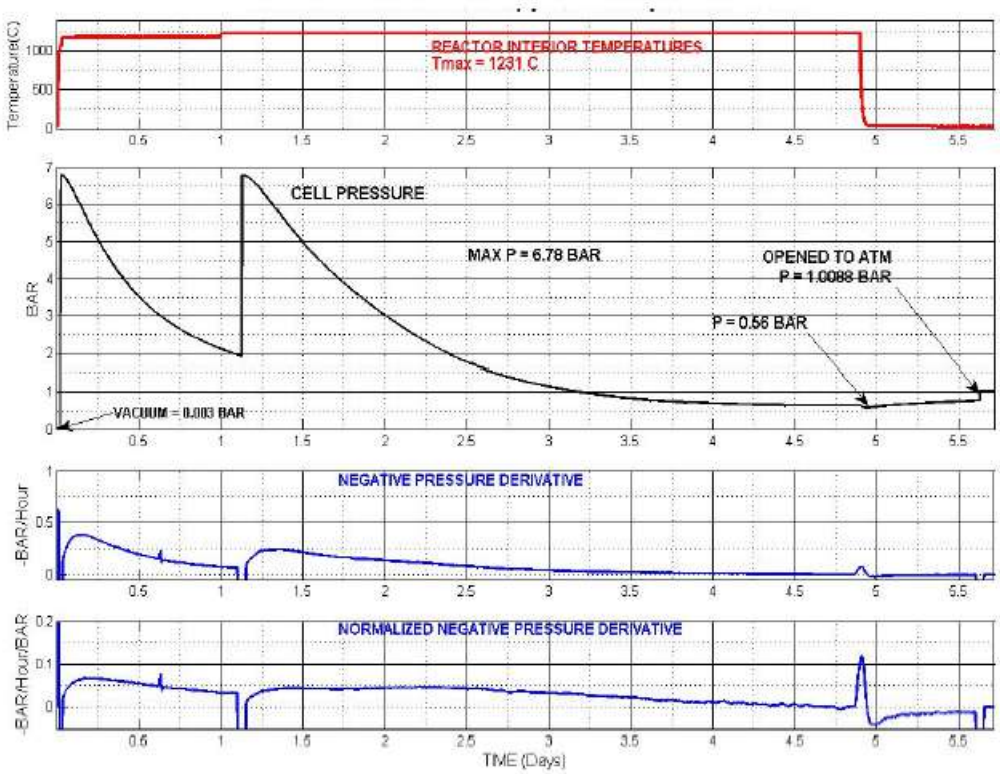

Figure 10. Pressurization of an empty cell.

cm of (0.635 cm OD) stainless tubing at room temperature. This is found to be 3.7×10^{-7} bar/h and thus is not a factor. Alumina permeation by hydrogen has been measured [9]. Using the alumina surface area, wall thickness, and pressures of the experiment and a temperature of 1250°C, a permeation rate of 0.004 bar/h is calculated. This is less than 1% of the observed rate.

For completeness, it is noted that the alumina tube is sealed to a stainless steel fitting using a sealant (Torr Seal) designed for vacuum systems. After a cell is fabricated but before it is used, it is pressurized with 100 psig (7.8 bar) of hydrogen, sealed with a valve, and monitored for a minimum of 24 h at room temperature. If no pressure drop is observed within the resolution of the Bourdon gauge (0.5 psi), the cell is considered leak free.

Because a high temperature could compromise the integrity of the stainless steel-alumina seal, the maximum temperature at the end of the alumina tube sealed with Torr Seal was measured. It was found to be 80°C when the interior temperature of the tube at the location of the nickel is 1250°C. This temperature was measured with the copper end-cap of the calorimeter that holds the stainless steel-alumina seal NOT in contact with the calorimeter (due to the leads of the thermocouples). Thus this end cap reached a considerably higher temperature than when it was used in the previous measurements and consequently it is unlikely that the Torr Seal reached 80° C during the measurements shown in Figs. 9 and 10. Torr Seal can be used "at temperatures from –45°C to 120°C (bakeable temperature)" [10]. Thus the sealant was significantly below the maximum operating temperature recommended by the manufacturer. One possibility not yet explored is absorption by the ceramic fiber in the end of the tube. Its composition is "high purity

alumina, zirconia and silica spun ceramic fibers" [6].

Although the data cited above [9] indicates that absorption into the tube is not the cause of these pressure drops, extended periods at high temperatures of the data in Figs. 9 and 10 or a difference alumina grades could make this data comparison invalid. At this writing this pressure drop is a topic of investigation.

Acknowledgements

We thank Drs. Jacques Ruer and Michael R. Staker for enlightening discussions.

References

[1] A.G. Parkhomov and E.O. Belousova, Research into heat generators similar to high-temperature Rossi reactor, *J. Condensed Matter Nucl. Sci*. **19** (2016) 244–256.
[2] An English translation of Parkhomov results using a flowing calorimeter can be found at https://drive.google.com/file/d/0Bz7lTfqkED9Wdm1NeEtxMFJLTmM/view.
[3] B.-J. Qi, M. He, S.-Y. Wu, Q.-Z. Zhao, X.-M. Wang, Y.-J. Pang, X.-L. Yang and S.-S. Jiang (jiang@ihep.ac.cn), Anomalous heat production in hydrogen-loaded metals: possible nuclear reactions occurring at normal temperature, China Institute of Atomic Energy, P.O. 275 (49), Beijing 102413.
[4] AdValue Technology Alumina Tube–Closed One End; 3/8-1/4-12 AL-T-N3/8-N1/4-12-COE; http://www.advaluetech.com/index.html.
[5] Novamet Specialty Products Corp., 1420 Toshiba Drive, Suite E, Lebanon, TN 37087, USA.
[6] Ceramic Blanket 2600, Thermal Products Co. Inc., 4520 S. Berkeley Lake Road, Norcross, GA 30071.
[7] Sun Xiukui, Xu Jian and Li Yiyi, Hydrogen permeation behaviour in austenitic stainless steels, *Matls Sci. Eng*. A **114** (1989) 179–187.
[8] E. Hashimoto and T. Kino, hydrogen permeation through Type 316 stainless steels and ferritic steel for a fusion reactor, *J. Nucl.Matls*. **133**,**134** (1985) 289–291.
[9] R.M. Roberts, T.S. Elleman, H. Palmour III and K. Verghese, Hydrogen permeability of sintered aluminum oxide, *J. Am. Ceramic Soc*. **62** (1979) 495–499.
[10] Agilent Torr Seal Low Vapor Pressure Resin Sealant Data sheet, Agilent Technologies, 121 Hartwell Avenue, Lexington, MA 02421, USA, 2014.